*J. Fluid Mech.* (1999), *vol.* 386, *pp.* 213–232. Printed in the United Kingdom



# The influence of the downstream pressure on the shock wave reflection phenomenon in steady flows

By G. BEN-DOR[1], T. ELPERIN[1], H. LI[1] AND E. VASILIEV[2]

[1] Pearlstone Center for Aeronautical Engineering Studies, Department of Mechanical Engineering, Ben-Gurion University of the Negev, Beer-Sheva, Israel
[2] Department of Computational Mechanics, Volgograd University, Volgograd, Russia

(Received 14 May 1997 and in revised form 19 October 1998)

The effect of the downstream pressure (defined here as the wake pressure behind the tail of the reflecting wedge) on shock wave reflection in steady flows is investigated both numerically and analytically. The dependence of the shock wave configurations on the downstream pressure is studied. In addition to the incident-shock-wave-angle-induced hysteresis, which was discovered a few years ago, a new downstream-pressure-induced hysteresis has been found to exist. The numerical study reveals that when the downstream pressure is sufficiently high, an inverse-Mach reflection wave configuration, which has so far been observed only in unsteady flows, can be also established in steady flows. Very good agreement between the analytical predictions and the numerical results is found.

## 1. Introduction

As indicated by Ben-Dor (1991), two shock-wave-reflection configurations are possible in steady flows: regular reflection (RR) and Mach reflection (MR). They are shown in figures 1(*a*) and 1(*b*), respectively. The RR wave configuration consists of two shock waves: the incident shock wave, i, and the reflected shock wave, r. They meet at the reflection point, R, which is located on the reflecting surface. The flow states are (0) ahead of i, (1) behind it, and (2) behind r. The angle of the incident shock wave, $\phi_1$, of a regular reflection is sufficiently small that the streamline deflection, $\theta_1$, caused by the incident shock wave can be cancelled by the opposite streamline deflection, $\theta_2$, caused by the reflected shock wave. Therefore, the boundary condition of a regular reflection is $\theta_1 - \theta_2 = 0$. The MR wave configuration consists of three shock waves: the incident shock wave, i, the reflected shock wave, r, and the Mach stem, m; and one slipstream, s. They all meet at a single point, the triple point, T. The Mach stem is usually a curved shock wave which is perpendicular to the line of symmetry at the reflection point R. The flow states are (0) ahead of i and m, (1) behind i, (2) behind r, and (3) behind m. Unlike the case of an RR where the net deflection of the streamline is zero, in the case of an MR the net deflection of the streamline is not necessarily zero and as a result the streamlines behind the triple point can be directed towards the line of symmetry. Since the streamlines on both sides of the slipstream must be parallel, the boundary condition across the slipstream

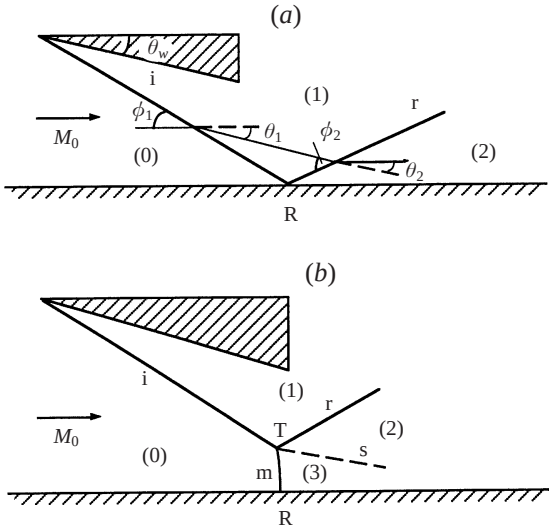


FIGURE 1. Schematic illustration of the wave configuration and definition of relevant parameters of (*a*) a regular reflection and (*b*) a Mach reflection.

of a Mach reflection is $\theta_1 - \theta_2 = \theta_3$, where $\theta_3$ is the streamline deflection caused by the Mach stem.

Two extreme angles of incidence, $\phi_1$, namely $\phi_1^N$, the von Neumann angle, and $\phi_1^D$, the detachment angle, at which the RR $\leftrightarrow$ MR transition can occur, are known. Theoretically, an RR wave configuration is not possible for $\phi_1 > \phi_1^D$ and an MR wave configuration is not possible for $\phi_1 < \phi_1^N$. In the range $\phi_1^N \leqslant \phi_1 \leqslant \phi_1^D$ both RR and MR wave configurations are theoretically possible. For this reason this range is known as the dual-solution domain.

The existence of the dual-solution domain led Hornung, Oertel & Sandeman (1979) to hypothesize that a hysteresis can exist in the RR $\leftrightarrow$ MR transition. Experimental attempts by Hornung & Robinson (1982), in a following study, to verify this hysteresis failed. The fact that there was no experimental evidence of this hypothesis led them, as well as all the other researchers, to believe that the RR wave configuration was unstable in the dual-solution domain.

Based on the principle of minimum entropy production, Li & Ben-Dor (1996*a*) showed analytically that the RR wave configuration is stable in almost the entire dual-solution domain. Soon after this, the hysteresis phenomenon in the RR $\leftrightarrow$ MR transition was recorded experimentally for the first time by Chpoun *et al.* (1995).† Then the existence of both RR and MR wave configurations in the dual-solution domain (for the same flow Mach numbers, $M_0$, and reflecting wedge angles, $\theta_w$, but different distances from the line of symmetry) was demonstrated numerically by Vuillon, Zeitoun & Ben-Dor (1995) using an FCT-based algorithm. Following these studies numerical simulations based on the DSMC method (Ivanov, Gimelshein & Beylich 1995; Ivanov *et al.* 1996, and Ben-Dor, Elperin & Golshtein 1997) and the

† Some researchers (see Hornung 1997 and references therein and Skews 1997) have been claiming that the experiments of Chpoun *et al.* (1995) were seriously contaminated by transverse flow effects (three-dimensional effects) and as a consequence should not be used as experimental evidence for proving the existence of hysteresis in a two-dimensional flow. The extent of these effects is yet to be studied and understood.

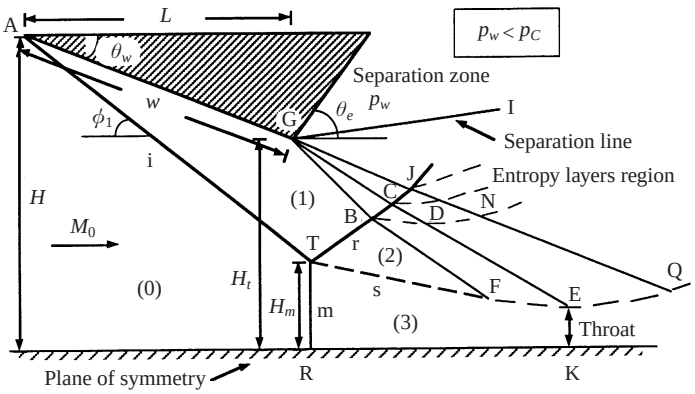


FIGURE 2. Schematic illustration of a Mach reflection wave configuration for the case $p_w < p_C$ and definition of relevant parameters; $p_w$ is the downstream pressure and $p_C$ is the pressure at point C.

TVD algorithm (Ivanov *et al.* 1996, and Shirozu & Nishida 1995) demonstrated the hysteresis phenomenon, for identical initial conditions.

Both Vuillon *et al.* (1995) in their numerical study and Chpoun *et al.* (1995) in their experimental study clearly demonstrated that the MR wave configuration depends on the geometrical parameters associated with the experimental set-up. This dependence, which was first suggested by Henderson & Lozzi (1979) and later by Hornung & Robinson (1982), was recently verified in Li & Ben-Dor's (1997) analytical investigation of the shock wave reflection in steady flows. Their analysis was limited to the case in which the triple point of the MR wave configuration was free of downstream influences. Li & Ben-Dor (1996*a*) assumed a similar limitation when they applied the principle of minimum entropy production to understand better the stability of shock wave reflections in steady flows. These findings together with Henderson & Lozzi's (1979) conclusion that the 'transition between RR and MR can be promoted or suppressed anywhere in the range $\phi_1^N \leqslant \phi_1 \leqslant \phi_1^D$ by suitable choice of downstream boundary conditions' were the motivation for our decision to conduct analytical and numerical studies, in order to understand better how the downstream pressure affects shock wave reflection in steady flows. Preliminary findings of this study which were reported recently by Ben-Dor *et al.* (1997*a*) revealed a downstream-pressure-induced hysteresis. Note that the term downstream pressure in this study does not refer to the pressure downstream on the centreline but to the wake pressure behind the wedge. Consequently, the aim of this study was to better understand this downstream-pressure-induced hysteresis by investigating it both analytically and numerically.

## 2. The analytical study

### 2.1. *The flow field analysis*

We begin by introducing the governing equations for the case in which the triple point of the Mach reflection is isolated from downstream effects. As will be shown subsequently, this is the case as long as the downstream pressure, $p_w$, is smaller than the pressure at point C which is defined in figure 2. A two-dimensional analytical study of this case was presented recently by Li & Ben-Dor (1997).

A detailed Mach reflection wave configuration together with the definition of relevant parameters is shown in figure 2. As mentioned earlier the MR wave configuration

consists of an incident shock, i, a reflected shock, r, a slightly curved Mach stem, m, and a contact surface (slipstream), s. The flow immediately behind the Mach stem (which is nearly a normal shock wave) is subsonic. The Mach stem must be perpendicular to the plane of symmetry at its foot, point R. The interaction of the reflected shock wave, r, with the centred expansion fan which emanates from the trailing edge of the shock-generating wedge (point G) results in a transmitted-reflected shock wave, r′, transmitted expansion waves and an entropy-layers region. Details of the analysis of the interaction of a shock wave with an expansion fan can be found in Li & Ben-Dor (1996*b*). The transmitted expansion waves which interact with the slipstream, s, cause the pressure in region (3), to drop in the streamwise direction. This in turn accelerates the flow to a supersonic condition. As a result, the cross-sectional area of the streamtube formed by the slipstream and the plane of symmetry decreases first to a minimum at which the flow reaches sonic conditions, and then increases again in the region of accelerating supersonic flow. A subsonic pocket, bounded by TFEKRT, is therefore formed in an otherwise supersonic flow. The flow downstream of the line GCDEK is supersonic, and hence is isolated from the subsonic pocket. The size and shape of this pocket (eventually the Mach stem height) are solely controlled by the length $w$ of the upper boundary of region (1) and the distance, $H_t$, between the trailing edge of the reflecting wedge and the plane of symmetry. It should be noted here that the concept that the sonic throat downstream of the Mach stem determines the position of the Mach stem was first mentioned by Hornung & Robinson (1982).

Li & Ben-Dor (1997) analytically predicted the normalized Mach stem height, $H_m/w$, and obtained, for the case in which the flow field is free of the downstream-pressure influences, a dependence of the form

$$H_m/w = f(\gamma, M_0, \theta_w, H_t/w), \tag{1}$$

where $\gamma, M_0, \theta_w, H_m, H_t$ and $w$ are the specific heats ratio, the incoming flow Mach number, the reflecting wedge angle, the Mach stem height, the exit cross-sectional area at the trailing edge, and the length of reflecting wedge, respectively.

### 2.2. *The governing questions*

For the flow field described in § 2.1, the Mach reflection wave configuration does not depend on the flow parameters in the regions downstream of the line GCDEK (see figure 2) provided it is free of downstream influences. Consequently, only the governing equations for solving the relevant flow regions shown in figure 2 are needed and presented in the following. For clarity the part of the figure showing the flow field relevant to the following discussion is shown enlarged in figure 3.

The region GBC is a Prandtl–Meyer fan, therefore

$$\nu(M_C) - \nu(M_1) = \theta_w - \alpha \tag{2}$$

and

$$p_C = p_1 \left[\frac{2 + (\gamma - 1)M_1^2}{2 + (\gamma - 1)M_C^2}\right]^{\gamma/(\gamma-1)}, \tag{3}$$

where $M_C$ and $p_C$ are the flow Mach number and the pressure along the characteristic GC, $\alpha$ is the flow direction relative to the horizontal direction, and $\nu(M)$ is the Prandtl–Meyer function, i.e.

$$\nu(M) = \left(\frac{\gamma+1}{\gamma-1}\right)^{1/2} \arctan\left[\frac{(\gamma-1)(M^2-1)}{\gamma+1}\right]^{1/2} - \arctan(M^2-1)^{1/2}. \tag{4}$$

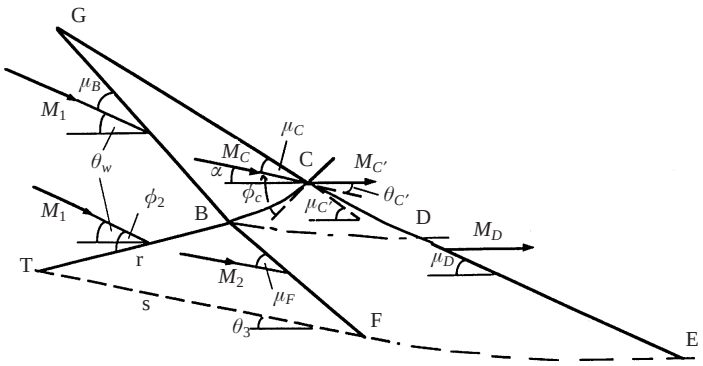


FIGURE 3. Enlargement of a section of the schematic drawing shown in figure 2 and definition of relevant parameters.

Across the curved shock wave at point C, one gets

$$M_{c'} = F(\gamma, M_C, \phi_C), \tag{5}$$

$$\theta_{c'} = G(\gamma, M_C, \phi_C), \tag{6}$$

$$p_{c'} = p_c H(\gamma, M_C, \phi_c) \tag{7}$$

where $M_{C'}, \theta_{C'}$ and $p_{C'}$ are the flow Mach number, the flow deflection angle and the pressure immediately behind the curved reflected shock wave at point C, respectively. The functions $F$, $G$ and $H$ that relate the flow properties on both sides of an oblique shock wave are

$$M_j = F(\gamma, M_i, \phi_j) = \frac{\left\{1 + (\gamma-1)M_i^2 \sin^2\phi_j + \left[\tfrac{1}{4}(\gamma+1)^2 - \gamma \sin^2\phi_j\right] M_i^4 \sin^2\phi_j\right\}^{1/2}}{\left[\gamma M_i^2 \sin^2\phi_j - \tfrac{1}{2}(\gamma-1)\right]^{1/2}\left[\tfrac{1}{2}(\gamma-1)M_i^2 \sin^2\phi_j + 1\right]^{1/2}}, \tag{8}$$

$$\theta_j = G(\gamma, M_i, \phi_j) = \arctan\left[\frac{2\cot\phi_j(M_i^2 \sin^2\phi_j - 1)}{M_i^2(\gamma + \cos 2\phi_j) + 2}\right] \tag{9}$$

and

$$\frac{p_j}{p_i} = H(\gamma, M_i, \phi_j) = \frac{1}{\gamma+1}\left[2M_i^2 \sin^2\phi_j - (\gamma-1)\right], \tag{10}$$

where $M_i$ and $M_j$ are the flow Mach numbers ahead of and behind the oblique shock wave, respectively, $p_i$ and $p_j$ are the flow pressure ahead of and behind the oblique shock wave, respectively, $\phi_j$ is the angle of incidence and $\theta_j$ is the deflection angle.

In the region BCJNDB in figure 2 (which is known as an entropy region), there is a continuous change in the entropy as the reflected shock curves through the expansion fan, as well as a continuous change in the flow direction and the pressure. Although the entropy varies from one streamline to another it is constant along any arbitrarily chosen streamline, in this region, since it passes through an expansion wave region. One can, therefore, imagine the region BCJNDB to consist of an infinite number of such streamlines. Since the flow is steady, the streamlines (entropy layers) should be parallel downstream of the last characteristic JN, i.e. the flow directions are the same and the pressures are equal at points J and N. Similarly, the flow directions and the pressures at points C and D are also identical. This can be seen from the fact that the points C and D can eventually replace points J and N, respectively, by increasing

the downstream pressure $p_w$. Note that the flow properties at points C and D are independent of $p_w$. Therefore, the overall changes of the flow properties across the entire entropy-layer region result in a situation in which the flow directions at points C and D along the curve CD are parallel and the pressures, at these points, are the same, i.e.

$$\alpha = \theta_{C'} \tag{11}$$

and

$$p_{C'} = p_D, \tag{12}$$

where $p_D$ is the pressure at point D.

When the transmitted expansion waves reach the slipstream, s, they partially reflect from it and partially transmit through it. As shown in Appendix A of Li & Ben-Dor (1997), under the first-order approximation, the reflected expansion waves are very weak and hence can be neglected. This neglect is also justified by all available experimental evidence, to the best of the authors' knowledge. Thus, region BFED can be assumed to be a simple wave region. Consequently, the flow parameters along the lines BF and DE remain constant. At point E where the sonic throat is located, the flow direction should be parallel to the plane of symmetry (i.e. the $x$-axis). Again by using the Prandtl–Meyer relation one gets

$$\nu(M_D) - \nu(M_2) = \theta_3 \tag{13}$$

and

$$p_D = p_2 \left[ \frac{2 + (\gamma - 1)M_2^2}{2 + (\gamma - 1)M_D^2} \right]^{\gamma/(\gamma-1)}. \tag{14}$$

The set of equations (2), (3), (5) to (7) and (11) to (14) consists of nine equations with nine unknowns, i.e. $M_C, M_{C'}, M_D, p_C, p_{C'}, p_D, \phi_C, \theta_{C'}$ and $\alpha$. Consequently, it is complete provided all the other parameters are known, as indeed is the case.

### 2.3. *The free of downstream influence condition*

An inspection of the flow field shown in figure 2 clearly indicates that as long as the downstream pressure, $p_w$, is smaller than the pressure along the characteristic GCDE, say, $p_C$, the flow upstream of GCDEK is isolated from downstream effects, i.e. it cannot be affected by the downstream pressure, $p_w$. Furthermore, as long as $p_w < p_C$ the characteristic GCDE is independent of the angle of the trailing edge of the reflecting wedge, $\theta_e$ . As a result the throat of the converging nozzle formed by the slipstream and the plane of symmetry line is fixed at point E, and the Mach stem height is independent of the trailing-edge angle, $\theta_e$. This fact was recently verified by Ben-Dor *et al.* (1997*b*) both numerically and experimentally.

The foregoing discussion could be summarized by concluding that the size of the Mach reflection wave configuration, in general, and the height of its Mach stem, in particular, are independent of the downstream pressure as long as

$$p_w \leqslant p_C. \tag{15}$$

A schematic drawing of the Mach reflection wave configuration corresponding to this condition is shown in figure 2. The domains in which this configuration is either dependent on or independent of the downstream pressure, $p_w$, for a fixed incident angle $\phi_1 = 40^\circ$ in the $(p_w/p_0, M_0)$-plane are shown in figure 4. The solid boundary line separating these domains has been calculated using the present analytical model. The numerical points that are added to figure 4 will be discussed subsequently.

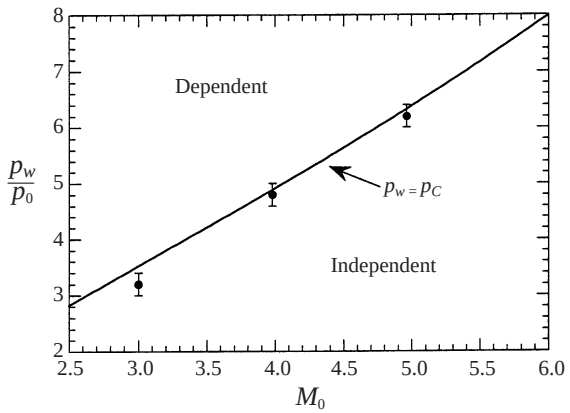


FIGURE 4. The domains in which a Mach reflection wave configuration is dependent on or independent of the downstream pressure in the $(p_w/p_0, M_0)$-plane for a fixed incident angle $\phi_1 = 40°$. The solid line shows the analytical prediction, the points the numerical calculations.

### 2.4. *The dependence on the downstream pressure*

When the downstream pressure, $p_w$, exceeds the pressure $p_C$ the Mach reflection wave configuration is no longer isolated from downstream effects: then, the value of the downstream pressure, $p_w$, with respect to the incident-shock-induced pressure, $p_1$, is the parameter controlling the flow field.

Schematic drawings of the Mach reflection wave configurations for three different cases are shown in figure 5. The case for which $p_1 > p_w > p_C$ is shown in figure 5(*a*). Unlike the Mach reflection shown in figure 2 for which $p_w < p_C$ here the throat is not formed by the primary expansion fan emanating from the trailing edge of the reflecting wedge but by a secondary expansion fan which results from the interaction of the free boundary of the separating zone, GG′, i.e. the separation line, with the transmitted-reflected shock wave, r′. (Details of the orientation of the separation line can be found in Schotz *et al.* 1997.)

An analytical model for calculating the interaction between the primary expansion fan, emanating from the trailing edge of the reflecting wedge, point G in figure 2, and the slipstream which result in the throat at point E was presented in detail by Li & Ben-Dor (1997). The model equations, together with the equations developed by Li & Ben-Dor (1998) when they dealt with an over-expanded supersonic nozzle, can be applied in a similar manner to calculate the interaction between the secondary expansion fan, emanating from point G′ in figure 5(*a*), and the slipstream which result in the throat at point E′.

The dependence of the normalized Mach stem height, $H_m/H$, on the downstream pressure, $p_w/p_0$, for $M_0 = 4.96$ and $\phi_1 = 40°$ as calculated using the present analytical model is shown in figure 6 (the numerical points, added to the figure, will be discussed subsequently). It is clearly evident that as long as $p_w \leqslant p_C$ the Mach stem height is constant as the entire MR wave configuration is isolated from downstream effects.

Once the downstream pressure, $p_w$, exceeds $p_C$ the Mach reflection is pushed upstream and as result its Mach stem height increases. The higher $p_w$ is the larger the Mach stem height becomes. The increase in $p_w$ causes the primary expansion fan to weaken until it practically vanishes when $p_w = p_1$. The wave configuration corresponding to this situation is shown in figure 5(*b*). The dependence of the normalized Mach stem height, $H_m/H$, on the angle of incident, $\phi_1$, for $M_0 = 4.96$ and

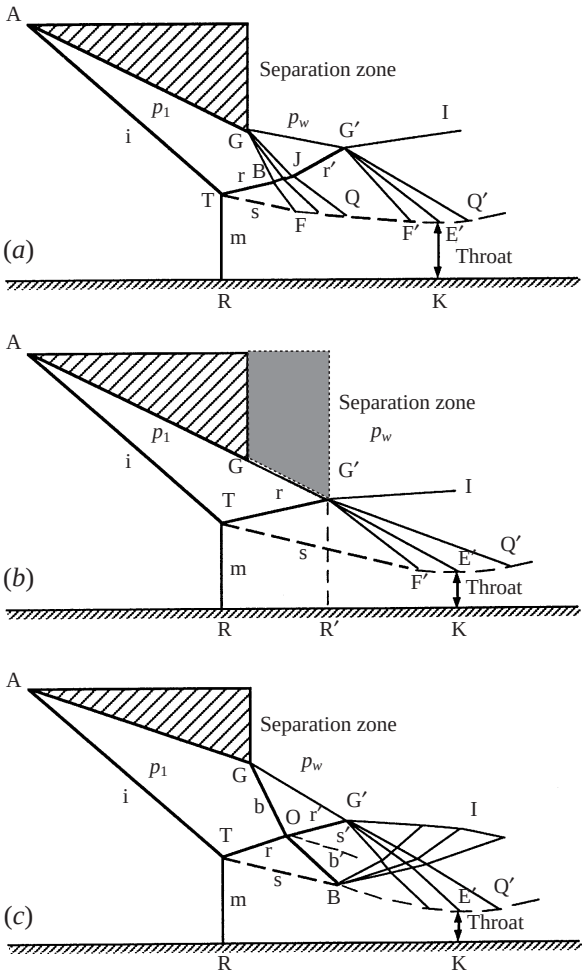


FIGURE 5. Schematic illustration of Mach reflection wave configurations for (*a*) $p_1 > p_w > p_C$, (*b*) $p_w = p_1$ and (*c*) $p_w > p_1$.

$p_w = p_1$ is shown in figure 7. It is clearly evident from this figure that the Mach stem vanishes, i.e. $H_m \to 0$, at $\phi_1 = 30.9°$, in perfect agreement with the von Neumann MR → RR transition angle.

It is also important to note that G′R′, in figure 5(*b*), is the minimum distance for which the flow in the nozzle, formed by the reflecting wedge and the plane of symmetry, could be started. Hence the reflecting wedge could be extended as shown by the shadowed area without causing any change in the flow field. Any further extension of the wedge would result in a situation in which a supersonic flow cannot be established in the nozzle. (More details regarding this situation can be found in Vuillon *et al.* 1995 and Li & Ben-Dor 1997.)

When $p_w$ exceeds $p_1$, the wave configuration shown in figure 5(*c*) is obtained. Now a shock wave, GO, rather than an expansion fan emanates from the trailing edge of the reflecting wedge. The throat is formed in a way similar to that shown in figure 5(*a*), i.e. by the expansion fan which results in from the interaction between the free boundary of the separation zone and the transmitted-reflected shock wave.

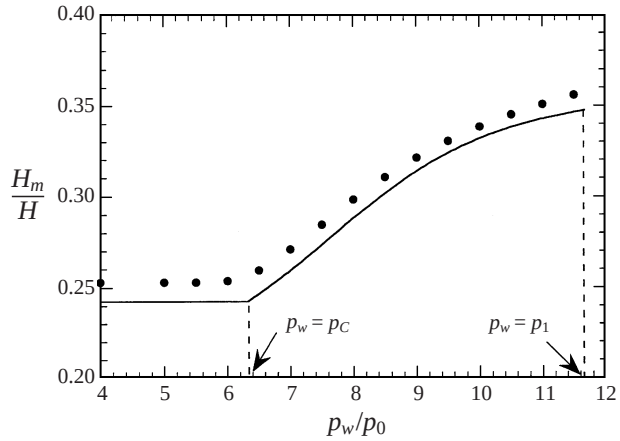


FIGURE 6. The dependence of the normalized Mach stem height, $H_m/H$, on the downstream pressure, $p_w/p_0$, for $M_0 = 4.96$ and $\phi_1 = 40°$. The solid line is the analytical prediction, the points are numerical calculations.

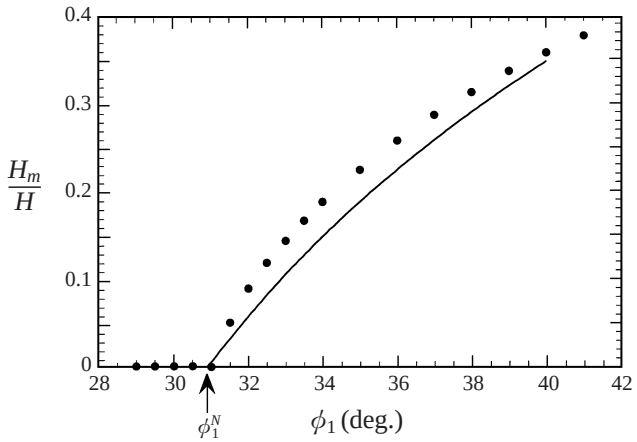


FIGURE 7. The dependence of the normalized Mach stem height, $H_m/H$, on the angle of incidence, $\phi_1$, for $M_0 = 4.96$ and $p_w = p_1$. The solid line is the analytical prediction, the points are numerical calculations. Note that based on the solid line $H_m \to 0$ exactly at the von Neumann condition $\phi_1 = \phi_1^N$.

Unfortunately, the flow field associated with the wave configuration shown in figure 5(*c*) is more complicated that those shown in figures 5(*a*) and 5(*b*), and hence an analytical solution of this Mach reflection wave configuration is not available yet.

## 3. The numerical study

### 3.1. *The numerical method*

During the last decade explicit monotonic schemes of high-order accuracy employing essentially nonlinear difference schemes have been widely used in computational fluid dynamics. The principal concept employed in the overwhelming majority of these methods was the use of conservative flux corrections through the cell boundaries for a regular linear first-order scheme. The nonlinearity of these corrections and non-

uniform mesh used in the calculations rendered the well-known theorem of Godunov invalid (e.g. Hirsch 1990).

Using similar one-dimensional corrections for each of the spatial coordinates allows the construction of monotonic second-order-accurate methods for two-dimensional conservation laws employing either coordinate splitting schemes (e.g. Hirsch 1990, chapter 20) or predictor-corrector type schemes (e.g. Hirsch 1990, chapter 17). However, these methods are computationally expensive since they employ multistage computations at each time step. Attempts to cut the number of computational stages while preserving the one-dimensional corrections may reduce the accuracy of the scheme to a first order in time. This is acceptable for solving stationary problems but is inappropriate for treating truly non-stationary problems.

A new second-order-accurate in space and time modification of Godunov's scheme (e.g. Hirsch 1990, chapter 20) for a system of conservation laws which employs corrections at the two-dimensional stencil (W-modified Godunov's scheme) has been used in the present numerical calculations. For details see Vasiliev (1996). The scheme uses additive corrections to fluxes in the governing system of equations (Euler equations) with the subsequent employment of the first-order-accurate Godunov scheme to the modified system of equations (with corrections to the fluxes). It can be proved that such a procedure provides a second-order-accurate in space and time solution of the Euler equations. The method was realized on a W-stencil with orientation depending on the local flow velocity (eigenvalues of the matrices in the conservation laws). The method can be viewed as a combination of the van Leer and Harten schemes (van Leer 1979; Harten 1983). In the following only the general idea of the scheme is described. More details can be found in Vasiliev (1996).

Consider a system of hyperbolic equations written in a conservative form:

$$\frac{\partial \omega}{\partial t} + \frac{\partial f(\omega)}{\partial x} + \frac{\partial g(\omega)}{\partial y} = 0, \tag{16}$$

where $\omega(x, y, t)$ is an $m$-component vector and $f(\omega)$ and $g(\omega)$ are the vectors of the fluxes. Then, the first-order Godunov scheme applied to the modified equation:

$$\frac{\partial \omega}{\partial t} + \frac{\partial f(\omega + \alpha)}{\partial x} + \frac{\partial g(\omega + \beta)}{\partial y} = 0 \tag{17}$$

provides a second-order-accurate in space and in time solution of equation (16) if

$$\alpha = \frac{\Delta x}{2} \operatorname{sgn} \frac{\partial f(\omega)}{\partial \omega} \frac{\partial \omega}{\partial x} + \frac{\Delta t}{2} \frac{\partial \omega}{\partial t} \tag{18}$$

and

$$\beta = \frac{\Delta y}{2} \operatorname{sgn} \frac{\partial g(\omega)}{\partial \omega} \frac{\partial \omega}{\partial y} + \frac{\Delta t}{2} \frac{\partial \omega}{\partial t}. \tag{19}$$

The nonlinear approximation of the terms $\alpha$ and $\beta$ during the numerical solution is performed using a W-stencil with orientation depending on the flow velocities (i.e. eigenvalues of the matrices $\partial f(\omega)/\partial \omega$ and $\partial g(\omega)/\partial \omega$). It can be shown that the suggested selection of $\alpha$ and $\beta$ in the case of a scalar linear equation, ensures the monotonicity of the solution under the same values of the Courant number as the regular Godunov scheme.

In the calculations of the shock waves reflection and the hysteresis phenomenon (which will be presented subsequently) the W-modification of Godunov's scheme was used with an adaptive curvilinear grid which moved with the Mach stem. In order to resolve the incident shock wave, the Mach stem and the flow separation

line a front tracking technique was employed. (see Kraiko, Makarov & Tillyaeva 1980). The boundary condition $p = p_w$ was imposed on the flow separation line. The grid consisted of 200 cells in the horizontal and 100 cells in the vertical directions, respectively. The stationary solutions were calculated in the following way.

The downstream pressure, $p_w$, was varied in a piecewise constant manner. Namely, first the downstream pressure was set equal to the incident-shock-wave-induced pressure, $p_1$ (i.e. $p_w = p_1$) and kept constant at this value during the time interval $\Delta t_1$. Then $p_w$ was increased linearly, during the time interval $\Delta t_2$ by a value of $\Delta p_w$ and again kept constant at its new value during the time interval $\Delta t_1$. This procedure was repeated until the required downstream pressure value was reached. Then the sign of the pressure increment, $\Delta p_w$, was changed, and the process was repeated in the reversed direction until the initial downstream pressure (i.e. $p_w = p_1$) was attained. The linear time interval, $\Delta t_2$, was set equal to 200–300 time steps. The time interval $\Delta t_1$ was set much larger, i.e. several thousand time steps, in order to obtain a stationary solution. The attainment of the stationary solution was checked by numerically calculating both the norm of the difference between two solutions at consecutive time step and the velocity of the Mach stem.

The non-reflecting boundary conditions (see e.g. Hirsch 1990, pp. 344–401 and references therein) were employed at the exit. Since the flow above the slipstream is supersonic the influence of the boundary conditions on the solution was rather weak. Subsonic patches in the flow are located under the slipstream, and they alternate with supersonic patches. Therefore, even when the exit boundary lies inside a subsonic zone the perturbations from this zone penetrate upstream only to the nearest supersonic zone. Although under these circumstances even simple extrapolation boundary conditions would perform quite well, the non-reflecting boundary conditions were chosen since they result in a faster convergence towards the stationary solution.

### 3.2. *The numerical results*

*Case* 1: $p_w < p_1$

The Mach reflection wave configurations for $M_0 = 4.96, \phi_1 = 40°, \theta_e = 30°$ and 10 different values of $p_w/p_0$ are shown in figures 8(*a*) to 8(*j*). The free of downstream influence condition for this case is $p_w/p_0 \leqslant p_C/p_0 = 6.32$. In addition, since for this case $p_1/p_0 = 11.69$, for all the cases shown in figure 8 $p_w < p_1$, i.e. an expansion fan emanates from the trailing edge of the reflecting wedge.

An inspection of figures 8(*a*) to 8(*j*) clearly indicates that the Mach stem height remains constant as long as $p_w \leqslant p_C$ in perfect agreement with the analytical predictions of the previous sections. Once $p_w$ exceeds $p_C$ the triple point is pushed upstream and the Mach stem height increases.

Figures 8(*a*) to 8(*j*) also illustrate how the primary expansion fan emanating from the trailing edge of the reflecting wedge weakens as the downstream pressure increases. While a very wide expansion fan is seen in figure 8(*a*), they progressively become narrower as the downstream pressure increases. Had the downstream pressure, $p_w$, exceeded $p_1$ the expansion fan would have been replaced by a shock wave as shown schematically in figure 5(*c*).

As a consequence of the weakening of the expansion fan the actual deflection of the flow around the trailing edge of the reflecting wedge decreases and the free boundary of the separation zone is seen to rotate in the clockwise direction. Note that while for $p_w/p_0 = 1$ (figure 8*a*) the separation line is almost horizontal, for $p_w/p_0 = 10$ (figure 8*j*) the separation line almost coincides with the surface of the reflecting wedge.

It should also be noted here that as a result of this rotation of the separation line, the

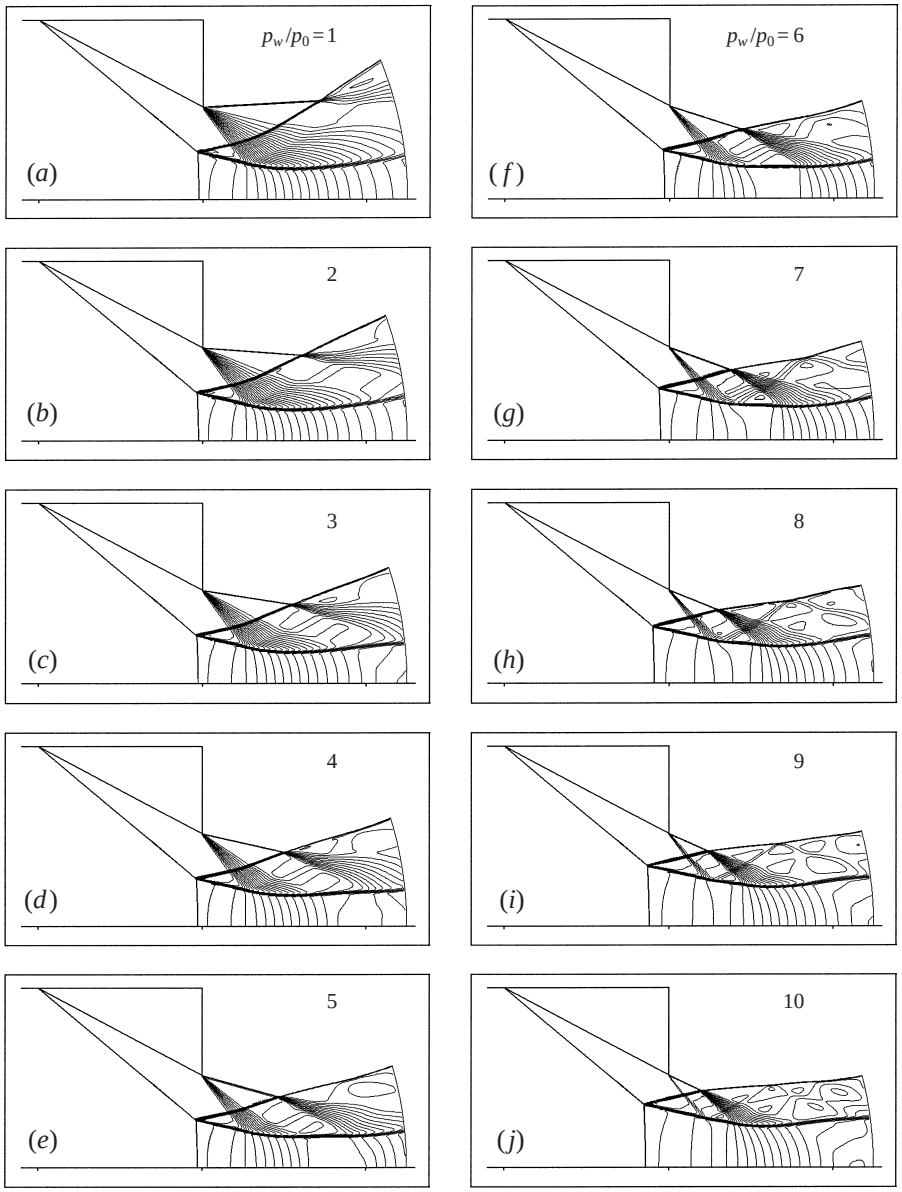


FIGURE 8. Numerical calculations of the density contours of Mach reflection wave configurations for $M_0 = 4.96$ and $\phi_1 = 40°(\theta_w = 28.21°)$, and ten different values of $p_w/p_0$; $H/L = 1.096$, Grid $200 \times 100$.

secondary expansion fan, i.e. the one resulting from the interaction of the separation line with the transmitted-reflected shock, becomes more and more dominant. While for $p_w/p_0 = 1$ (figure 8*a*) it does not interact with the slipstream, for $p_w/p_0 = 10$ (figure 8*j*) it is seen to have a strong influence on the slipstream shape in general and the location of the sonic throat in particular.

Note also that the flow field between the two expansion fans is almost uniform. It is only slightly perturbed by weak compression waves that result from the reflection of the primary expansion waves from the slipstream.

It is also evident from figure 8 that between $p_w/p_0 = 4$ (figure 8*d*) and $p_w/p_0 = 6$ (figure 8*f*) the flow field is uniform between the waves of the two expansion fans which penetrated through the slipstream. (An inspection of flow Mach number contours indicates that the flow field between these two expansion fans is supersonic. Hence the primary expansion fan is isolated from the secondary one through which information regarding the downstream pressure is communicated.) The slipstream between the tail of the primary expansion fan and the head of the secondary expansion fan is almost parallel to the plane of symmetry.

For $1 \leqslant p_w/p_0 \leqslant 6$ (figures 8*a* to 8*f*) the position of the Mach stem remained unchanged. However, as can be seen from figure 8(*g*) at $p_w/p_0 = 7$, the waves of the primary expansion fan are locked in the converging subsonic region of the flow downstream of the Mach stem. Thus, for this condition, the downstream pressure can influence the Mach reflection wave configuration, as indeed is the case in figure 8(*g*) where a small shift in the Mach stem location is evident. As the downstream pressure further increases (see figures 8*h* to 8*j*) the Mach stem shifts further upstream.

The normalized Mach stem heights as calculated numerically were added to the analytical prediction shown in figure 6. As can be seen the agreement between the analytical prediction and the numerical results is good; the difference could be attributed to the over-simplifying assumptions of the analytical model.

In order to better understand the mechanism generating the sonic throat in the flow field, the cases for $p_w/p_0 = 5, 6$ and 7, shown in figures 8(*e*) to 8(*g*), respectively, are redrawn in figures 9(*a*) to 9(*c*) using constant flow Mach number contours rather than constant density contours. Recall that the analytically predicted value of $p_C/p_0$ for this case is 6.32. For the reader's convenience, the subsonic patch in the flow field is shaded in figure 9. In the case shown in figure 9(*a*), for which $p_w/p_0 < p_C/p_0$ the sonic throat is formed by the primary expansion fan emanating from the trailing edge of the reflecting wedge in a way similar to that shown schematically in figure 2. On the other hand, in the case shown in figure 9(*c*), the sonic throat is formed by the secondary expansion fan that results from the interaction of the free surface of the separation zone with the transmitted-reflected shock wave in a way similar to that shown schematically in figure 5(*a*).

It is important to note that the kinks and undulations which are observed in the waves of the expansion fans are a result of their reflection from the slipstream. For explanatory purposes the case shown in figure 8(*h*) is redrawn in more detail in figure 10. Note that while the primary expansion fan reflects from the subsonic part of the slipstream as a compression wave, the secondary expansion fan reflects from the supersonic part of the slipstream as an expansion wave. The reflected compression and expansion fans interact with the primary and secondary expansion fans to result in a complex flow field. It is also evident from figure 10 that owing to the existence of a slight pressure gradient behind the Mach stem the flow field behind the reflected shock wave is not uniform.

*Case* 2: $p_w = p_1$

The wave configurations for $M_0 = 4.96, p_w = p_1$ and four different values of incident shock wave angle $\phi_1$ are shown in figures 11(*a*) to 11(*d*). The wave configurations in figures 11(*a*) to 11(*c*) where a Mach reflection is obtained are similar to the schematic illustration shown in figure 5(*b*). It is clearly evident that as $\phi_1$ decreases the Mach stem height decreases until a transition from Mach to regular reflection is obtained between $\phi_1 = 32^\circ$ and $30^\circ$.

The numerical results of the Mach stem height as a function of the angle of

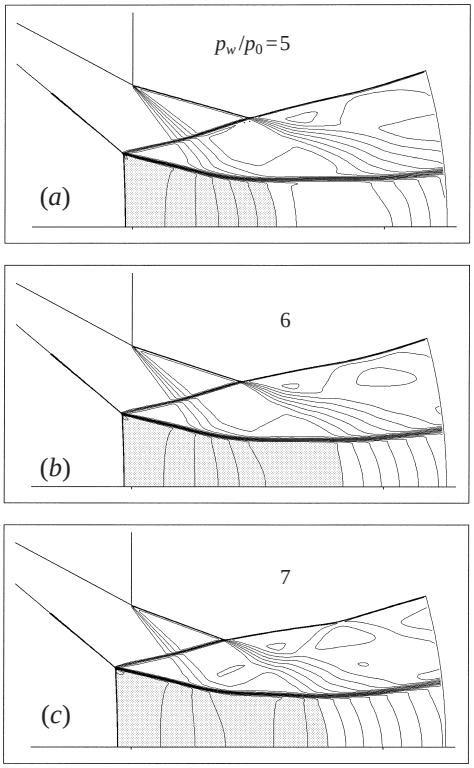


FIGURE 9. Numerical calculations of the flow Mach number contours of the three cases shown in figures 9(*e*) to 9(*g*).

incidence were added to figure 7. Both the analytical and the numerical results excellently predict the transition value. The reason why the analytical prediction of the transition is so good, for this case, is due to the fact that the over-simplifying assumptions in the analytical model become strictly valid when the Mach stem height approaches zero, i.e. $H_m \to 0$.

It is important to note that the kinks seen in the waves of the expansion fan are a results of its reflection from the slipstream. This interaction is similar to the one considered earlier (see figure 10).

*Case* 3: $p_w > p_1$

Numerical simulations for the case shown in figure 5(*c*), in which $p_w > p_1$ and hence a shock wave emanates from the trailing edge of the reflecting wedge, are shown in figures 12(*a*) to 12(*m*). The initial conditions for these simulations are $M_0 = 4.96$, $\phi_1 = 29.5^\circ$ and hence $p_1/p_0 = 6.79$. These results were obtained in the following way. First the case with $p_w/p_0 = 10 > p_1/p_0$ was solved. Then, the final results for $p_w/p_0 = 10$ were used as the initial conditions for $p_w/p_0 = 12$. This procedure was repeated until the value $p_w/p_0 = 22$ was reached. Then $p_w/p_0$ was decreased, again by using the final results of the previous case as the initial conditions for the next case until the value $p_w/p_0 = 10$ was reached again.

As can be seen from the results shown in figures 12(*a*) to 12(*m*) a hysteresis exists in the reflection phenomenon. While the transition from regular to Mach reflection was obtained between $p_w/p_0 = 18$ and 20 (see figures 12*e* and 12*f*), the reversed transition

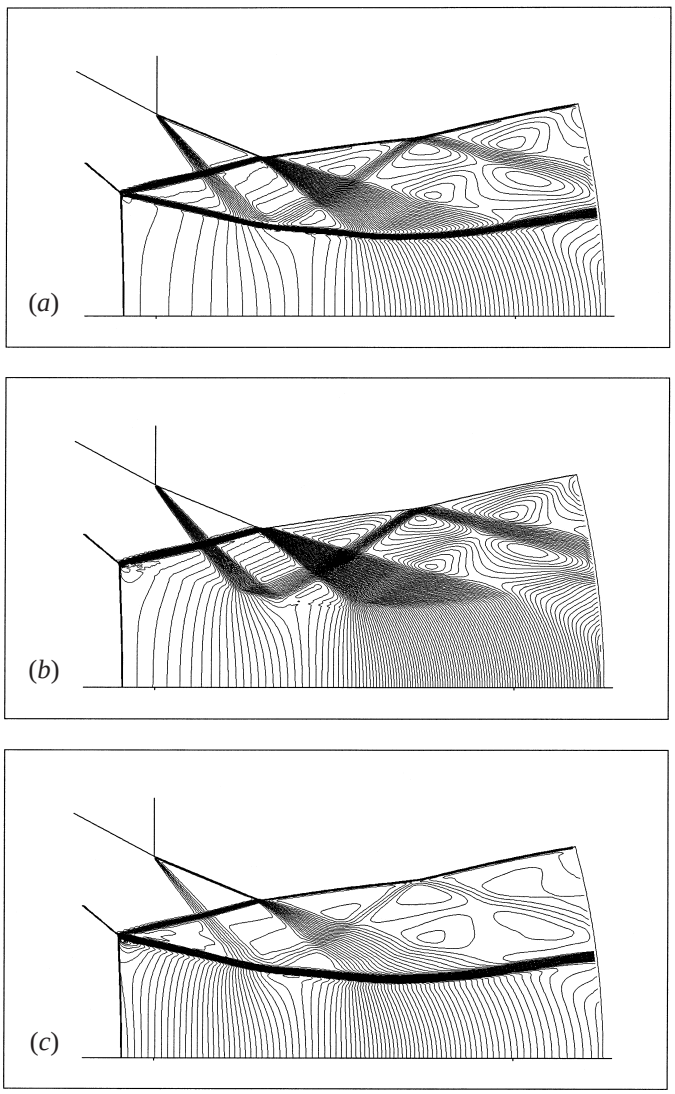


FIGURE 10. Detailed numerical results for (*a*) density, (*b*) pressure and (*c*) Mach number contours for the case shown in figure 8(*h*): $M_0 = 4.96$ and $\phi_1 = 40^\circ$ ($\theta_w = 28.21^\circ$), $p_w/p_0 = 8, H/L = 1.096$, Grid $200 \times 100$.

from Mach to regular reflection was obtained between $p_w/p_0 = 12$ and 10 (see figures 12*l* and 12*m*).

Figures 13(*a*) to 13(*e*) show the process between $p_w/p_0 = 18$ and 20 with smaller steps of 0.5 in $p_w/p_0$. Based on these simulations the transition from regular to Mach reflection occurs in the range $19.5 < p_w/p_0 < 20$. It is very important to note that the von Neumann angle for the flow conditions of the calculations shown in figures 12 and 13 is $\phi_1^N = 30.9^\circ$. Thus, based on the three-shock theory, a direct-Mach reflection wave configuration cannot be obtained for $\phi_1 < 30.9^\circ$. Consequently, the Mach reflection wave configurations shown in figures 12(*f*) to 12(*l*) and figure 13(*e*), for which $\phi_1 = 29.5^\circ < \phi_1^N$, are inverse-Mach reflections in which, unlike the configuration of a direct-Mach reflection such as that shown in figure 2, the slipstream

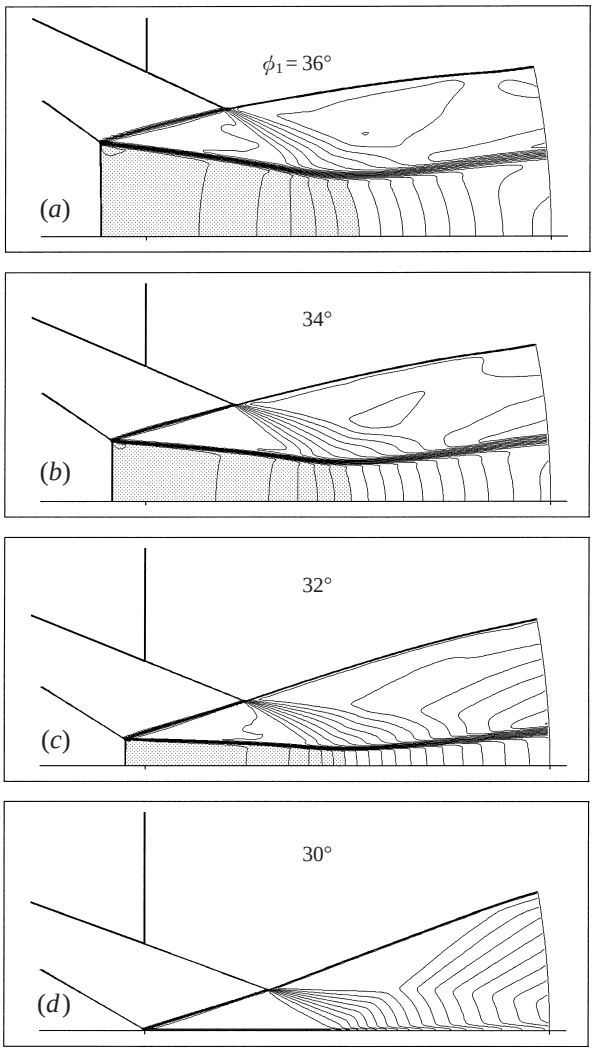


FIGURE 11. Numerical calculations of the flow Mach number contours of the wave configurations for $M_0 = 4.96, p_w = p_1$ and four different values of incident shock wave angle, $\phi_1$.

is directed away from the line of symmetry. For more details on the inverse-Mach reflection see Takayama & Ben-Dor (1985) and Ben-Dor & Elperin (1991). To the best of the authors' knowledge, inverse-Mach reflections have not been observed yet in the reflection of symmetric shock waves in steady flows.

The fact that Mach reflection wave configurations are obtained for $\phi_1 < \phi_1^N$ when the downstream pressure is sufficiently high can explain the experimental results of Hornung & Robinson (1982) which were not published directly by them but were reported by Azevedo (1989) who obtained the raw optical records from Hornung. These records clearly showed Mach reflection wave configurations in the domain $\phi_1 < \phi_1^N$ in which, theoretically, they are impossible.

As a final remark it should also be noted that the hysteresis shown in figures 12(*a*) to 12(*l*) is different from the hysteresis hypothesized by Hornung *et al.* (1979) and verified experimentally by Chpoun *et al.* (1995): while the hysteresis there was

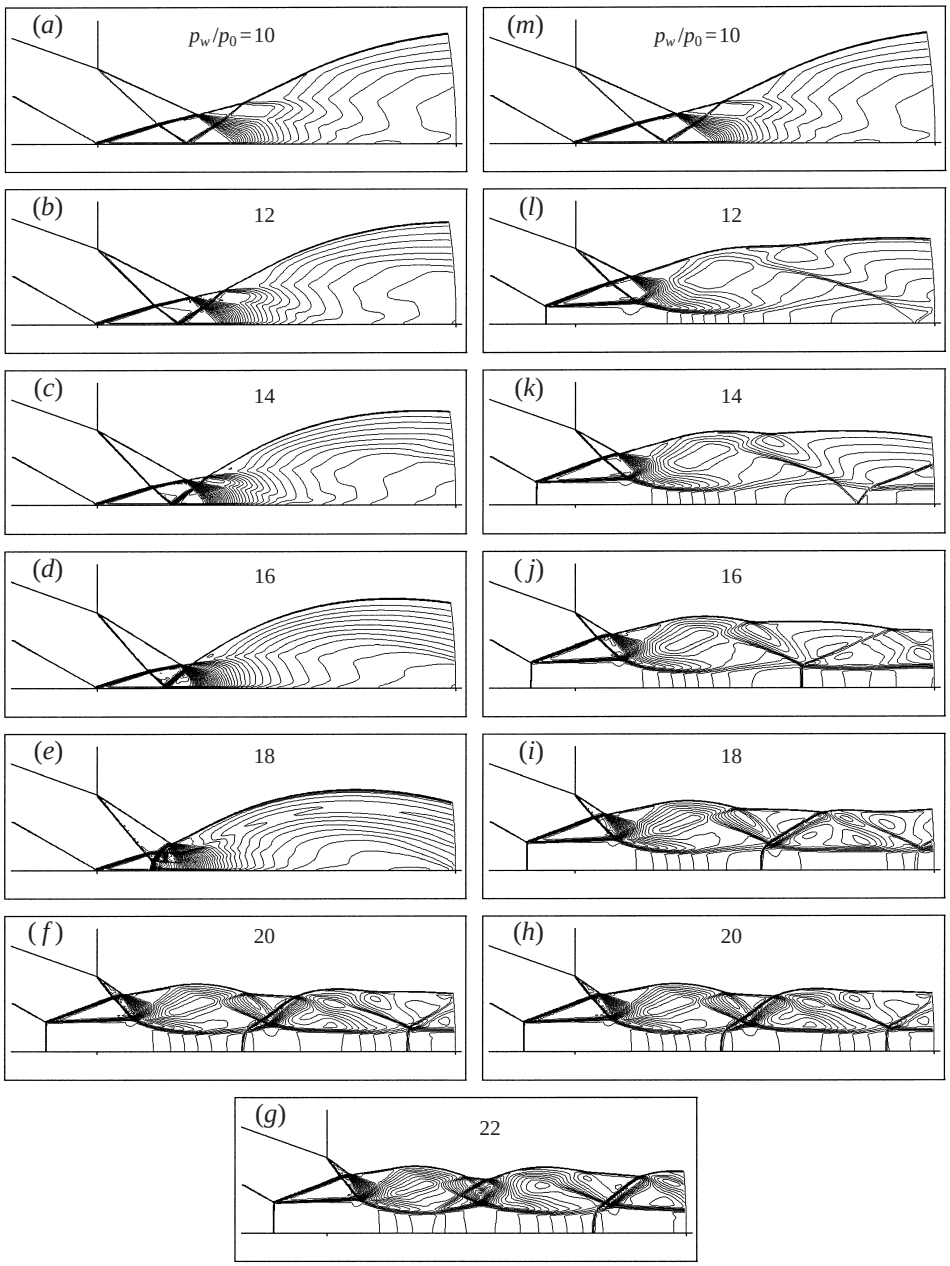


FIGURE 12. Numerical calculations of the density contours of the wave configurations for $M_0 = 4.96$ and $\phi_1 = 29.5°$ and thirteen different values of $p_w/p_0$. Note that in all the cases $p_w/p_0 > p_1/p_0$; $H/L = 0.566$, Grid $220 \times 60$.

incident-shock-wave-angle dependent the one shown here is downstream-pressure dependent.

The downstream-pressure-induced hysteresis loop is shown in figure 14 in the $(H_m/L, p_w/p_0)$-plane. As can be seen the MR $\rightarrow$ RR transition accurs at $p_w/p_0 = 19.63$ and the reverse RR $\rightarrow$ MR transition occurs at $p_w/p_0 = 10.00$. Both the MR $\rightarrow$ RR

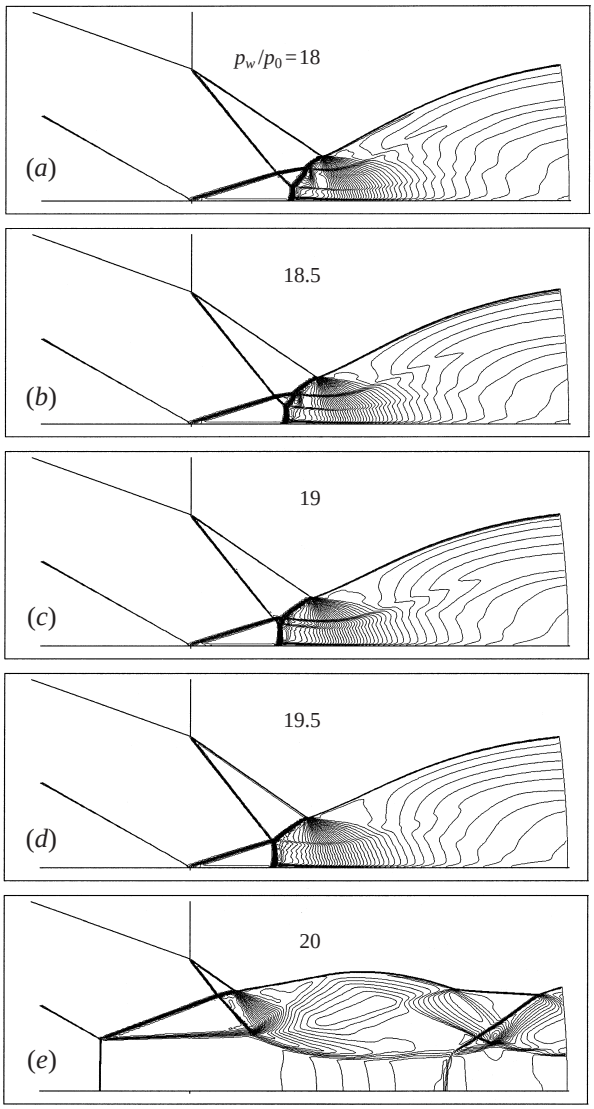


FIGURE 13. Numerical calculations of the density contours of the wave configurations for $M_0 = 4.96$ and $\phi_1 = 29.5°$ and five different values of $p_w/p_0$ which cover the range in which the transition from regular to Mach reflection takes place.

and the RR $\rightarrow$ MR transitions are associated with a sudden disappearance and appearance of a finite-size Mach stem.

## 4. Conclusions

Analytical and numerical investigations of the effect of the downstream pressure on the shock wave configuration in steady flows were conducted. The criterion for the reflection to be free of downstream-pressure effects was established. In addition, it was shown that depending on whether the downstream pressure is smaller than, equal to or larger than the incident-shock-induced pressure, three different wave configurations are possible. They differ in the type of wave emanating from the trailing edge of the

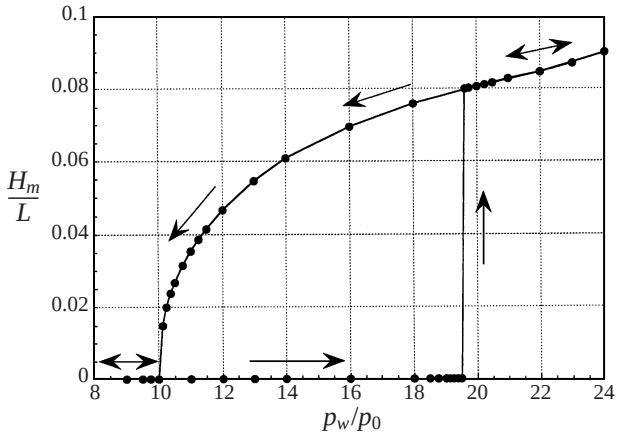


FIGURE 14. The downstream-pressure-dependent hysteresis loop in the $(H_m/L, p_w/p_0)$-plane. Note the sudden appearance of the Mach stem in the RR $\rightarrow$ MR transition at $p_w/p_0 = 19.32$.

reflecting wedge. When the downstream pressure was larger than the incident-shock-induced pressure the inverse-Mach reflection, which has not been observed so far in the reflection of symmetric shock waves in steady flows, was established.

The present results could probably be used to explain the hysteresis phenomenon which was recorded experimentally by Henderson & Lozzi (1979) using symmetric concave wedges. Owing to the fact that the wedges were concave the compression waves which emanated from their surfaces could have been the mechanism generating the high downstream pressure required to obtain the hysteresis with an inverse-Mach reflection.

The results of the present study could be useful in better understanding the stability of the flow through supersonic intakes, such as jet engines, which are exposed to either continuous or sudden (shock wave impact) changes of the surrounding pressure at their exits.

We acknowledge support for this research by the Israel Science Foundation, under Grant No. 173/95.

## REFERENCES

AZEVEDO, D. J., 1989 Analytic prediction of shock patterns in a high-speed wedge bounded duct. PhD thesis, Dept. Mech. & Aero. Engng, State Univ. NY Buffalo.

BEN-DOR, G. 1991 *Shock Wave Reflection Phenomena*. Springer.

BEN-DOR, G. & ELPERIN, T. 1991 Analysis of the wave configuration resulting from the termination of an inverse Mach reflection. *Shock Waves* **1**, 237.

BEN-DOR, G., ELPERIN, T. & GOLSHTEIN, E. 1997 Monte-Carlo analysis of the hysteresis phenomenon in steady shock wave reflection. *AIAA J.* **35**, 1777.

BEN-DOR, G., ELPERIN, T., LI, H. & VASILIEV, E. 1997*a* Downstream pressure induced hysteresis in the regular–Mach reflection transition in steady flows. *Phys. Fluids* **9**, 3096.

BEN-DOR, G., ELPERIN, T., LI, H., VASILIEV, E., CHPOUN, A. & ZEITOUN, D. 1997*b* Dependence of steady Mach reflections on the reflecting-wedge-trailing-edge-angle. *AIAA J.* **35**, 1780.

CHPOUN, A., PASSEREL, D., LI, H. & BEN-DOR, G. 1995 Reconsideration of oblique shock wave reflection in steady flows. Part 1. Experimental investigation. *J. Fluid Mech.* **301**, 19.

HARTEN, A. 1983 High resolution schemes for hyperbolic conservation laws. *J. Comput. Phys.* **49**, 357.

Henderson, L. F. & Lozzi, A. 1979 Further experiments on transition to Mach reflection. *J. Fluid Mech.* **94**, 541.

Hirsch, C. 1990 *Numerical Computation of Internal and External Flows.* John Wiley.

Hornung, H. G. 1997 On the stability of steady-flow regular and Mach reflection. *Shock Waves* **7**, 123.

Hornung, H. G., Oertel, H. Jr. & Sandeman, R. J. 1979 Transition to Mach reflection of shock waves in steady and pseudo steady flow with and without relaxation. *J. Fluid Mech.* **90**, 541.

Hornung, H. G. & Robinson, M. L. 1982 Transition from regular to Mach reflection of shock waves. Part 2. The Steady-flow criterion. *J. Fluid Mech.* **123**, 155.

Ivanov, M. S., Gimelshein, S. F. & Beylich, A. E. 1995 Hysteresis effect in stationary reflection of shock waves. *Phys. Fluids* **7**, 685.

Ivanov, M. S., Zeitoun, D., Vuillon, J., Gimelshein, S. F. & Markelov, G. 1996 Investigation of the hysteresis phenomena in steady shock reflection using kinetic and continuum methods. *Shock Waves* **5**, 341.

Kraiko, A. N., Makarov, V. E. & Tilyeva, N. N. 1980 On the numerical construction of shock-wave fronts. *J. Comput. Maths Math. Phys.* **20**, 181.

Leer, B. van 1979 Towards the ultimate conservative difference scheme. V. A Second order sequel to Godunov's method. *J. Comput. Phys.* **32**, 101.

Li, H. & Ben-Dor, G. 1996*a* Application of the principle of minimum entropy production to shock wave reflections. I. Steady flow. *J. Appl. Phys.* **80**, 2027.

Li, H. & Ben-Dor, G. 1996*b* Oblique-shock/expansion-fan interaction: Analytical solution. *AIAA J.* **34**, 418.

Li, H. & Ben-Dor, G. 1997 A parametric study of Mach reflection in steady flows. *J. Fluid Mech.* **341**, 101.

Li, H. & Ben-Dor, G. 1998 Mach reflection wave configurations in two-dimensional supersonic jets of overexpanded nozzles. *AIAA J.* **36**, 488.

Schotz, M., Levy, A., Ben-Dor, G. & Igra, O. 1997 Analytic prediction of the wave configuration size in steady flow Mach reflections. *Shock Waves* **7**, 363.

Shirozu, T. & Nishida, M. 1995 Numerical studies of oblique shock reflection in steady two-dimensional flows. *Mem. Faculty Engng, Kyushu University, Fukuoka, Japan* **55**, 193.

Skews, B. W. 1997 Aspect ratio effects in wind tunnel studies of shock wave reflection transition. *Shock Waves* **7**, 373.

Takayama, K. & Ben-Dor, G. 1985 The inverse Mach reflection. *AIAA J.* **23**, 1853.

Vasiliev, Ye. I. 1996 A W-modification of Godunov's method and its application to two-dimensional non-stationary flows of a dusty gas. *Comput. Maths Math. Phys.* **36**, 101.

Vuillon, J., Zeitoun, D. & Ben-Dor, G. 1995 Reconsideration of oblique shock wave reflection in steady flows. Part 2. Numerical investigation. *J. Fluid Mech.* **301**, 37.